COMMUNICATIONS PHYSICS

ARTICLE

https://doi.org/10.1038/s42005-020-0293-7 OPEN

Cold clouds as cosmic-ray detectors

Shmuel Bialy [1*]

Low energy cosmic-rays (CRs) are responsible for gas heating and ionization of interstellar clouds, which in turn introduces coupling to Galactic magnetic fields. So far the CR ionization rate (CRIR) has been estimated using indirect methods, such as its effect on the abundances of various rare molecular species. Here we show that the CRIR may be constrained from line emission of H_2 rovibrational transitions, excited by CRs. We derive the required conditions for CRs to dominate line excitation, and show that CR-excited lines may be detected with the Very Large Telescope (VLT) over 8 hours integration. Our method, if successfully applied to a variety of clouds at different Galactic locations, will provide improved constraints on the spectrum of low energy CRs and their origins.

[1] Harvard Smithsonian Center for Astrophysics, 60 Garden st., Cambridge, MA 02138, USA. *email: sbialy@cfa.harvard.edu

The ionization fraction of atomic and molecular clouds is a primary factor in determining the gas evolution: it determines the efficiency of heating and cooling processes, drives the chemistry and molecule formation, and enables coupling to Galactic magnetic fields. Ultraviolet (UV) radiation from starlight provides gas ionization, but this is restricted to localized regions, exposed to intense fluxes in the vicinity of massive stars. For the bulk of the gas in the Galaxy, the ionization is governed by cosmic-rays (CRs) (see ref. [1] for a review).

It is the low energy CRs ($E \ll$ GeV) that is responsible for gas ionization in the interstellar medium (ISM), however, direct observations from Earth may only probe high energy CRs. Over the past few decades, the CR ionization rate (CRIR), denoted ζ (hereafter ζ is the total number of H_2 ionization per molecule, per sec, including both ionizations by CRs and by the secondary electrons produced by CR ionization), was estimated through observations of various molecules and molecular ions in the ISM, such as OH, OH^+, H_2O^+, H_3^+, ArH^+, etc. When combined with chemical models, these observations constrain the CRIR, yielding typical values ranging from $\zeta = 10^{-17}$ to $10^{-15}\,s^{-1}$ in dense and diffuse Galactic clouds[2–7], and up to $\zeta \approx 10^{-14}\,s^{-1}$ in the Galactic center[8] and in extragalactic sources[9–11].

However, these determinations rely on the abundances of secondary species and depend on various model assumptions. For example, the gas density, the rate coefficients of the chemical reaction, the fractional abundances of H_2, e^-, O, CO, etc., the number of clouds along the line-of-sight[12,13]. Other indirect methods for inferring the CRIR include the analysis of the thermal balance of dust and gas[14–16], the effect on deuterium fractionation[17–20], and through radio recombination lines[21,22] and synchrotron radiation[23].

The mass of molecular clouds in the ISM is strongly dominated by H_2. The gas in molecular clouds is typically cold and the H_2 molecules reside mostly in their ground electronic, vibrational and rotational configuration. However, H_2 rotational and vibrational transitions have been previously observed in shocked warm gas ($T \gtrsim 1000$ K), where the H_2 levels are thermally excited. H_2 emission lines are also routinely observed in bright photon-dominated regions (PDRs), in which the H_2 is excited by UV pumping[24–26]. These regions are exposed to abnormally high UV fluxes, $\chi \gg 1$, where χ is the radiation intensity normalized to the mean interstellar radiation field[27]. As we show below, for the more typical conditions of molecular gas in the ISM, i.e., cold ($T \lesssim 100$ K) and quiescent ($\chi \approx 1$), CRs are expected to dominate H_2 excitation.

Numerical computations for H_2 excitation by energetic electrons were presented by[28,29]. Excitation by UV photons has been discussed by[30–32], and the excitation through the H_2 formation process, has been the focus of refs. [33–35].

In this paper, we show that the CRIR may be determined through observations of line-emission from the main constituent of the cloud mass, H_2. The H_2 rovibrational levels are excited by interactions with energetic electrons, which are produced by CR ionization. As they radiatively decay they produce line emission in the infrared (IR) that is $\propto \zeta$. We adopt an analytic approach to quantify the conditions required for robust detection of H_2 lines that are excited by CRs: (a) we consider the various line excitation mechanisms and their dependence on astrophysical parameters and derive the critical ζ/χ above which CR excitation dominates line emission over UV and formation pumping, and (b) consider the feasibility of line detection above the continuum with state of the art instruments.

Results

Cosmic-ray pumping. We consider the emission of H_2 vibrational transitions from cold molecular clouds, where the vibrational levels are excited by penetrating CRs (and secondary electron). As we discuss below, the line brightness is proportional to the CRIR, and thus may be used to constrain the CRIR inside clouds. Because radiative decay rates are high compared to the excitation rates, any excitation quickly decays back to the initial ground state before encountering the next excitation. Therefore, it is possible to separate the contribution from various excitation processes: CR excitation, UV excitation, and excitation following H_2 formation, (as discussed in the following subsections). We focus on cold $T \lesssim 50$ K gas typical of dense molecular cloud interiors. In Methods we discuss warmer gas and the dependence of the line intensities on temperature.

Assuming that the H_2 reside in the ground vibrational ($v = 0$, J) states and that each vibrational excitation is rapidly followed by radiative decay (see Methods), the surface brightness of a transition line is

$$I_{ul,(\mathrm{cr})} = \frac{1}{4\pi} g N_{\mathrm{H}_2} \zeta_{\mathrm{ex}} p_{u,(\mathrm{cr})} \alpha_{(u)l} E_{ul}, \tag{1}$$

where u and l denote the upper and lower energy states of the transition and

$$g(\tau) \equiv \frac{1 - \mathrm{e}^{-\tau}}{\tau} \approx \frac{1 - \mathrm{e}^{-0.9 N_{22}}}{0.9 N_{22}} \tag{2}$$

accounts for dust extinction in the infrared. $\tau = \sigma_d N$ is the optical depth for dust extinction, and $\sigma_d \approx 4.5 \times 10^{-23}\,\mathrm{cm}^2$ is the cross-section per hydrogen nucleus (the numeric value is an average over 2–3 μm[36]), where N_{H_2} and $N \approx 2N_{\mathrm{H}_2}$ are the column densities of H_2 and hydrogen nuclei, and $N_{22} \equiv N_{\mathrm{H}_2}/(10^{22}\,\mathrm{cm}^{-2})$. In the limit $\tau \ll 1$, $g \to 1$ and $I_{ul,(\mathrm{cr})} \propto N_{\mathrm{H}_2}$, i.e., the optically thin limit. In the limit $\tau \gg 1$, $I_{ul,(\mathrm{cr})}$ saturates as $g N_{\mathrm{H}_2} \to 1/(2\sigma_d) = 1.1 \times 10^{22}\,\mathrm{cm}^{-2}$. This is the optically thick limit. For typical conditions, $N_{22} = 1$, $\tau = 0.9$, and $g \approx 0.66$. $\zeta_{\mathrm{ex}} \propto \zeta$ is the total excitation rate by CRs and by secondary electrons, and $p_{u,(\mathrm{cr})}(T)$ is the probability per CR excitation to excite level u, as determined by the interaction cross-sections for CRs and $H_2(v = 0, J)$, assuming the rotational levels of $H_2(v = 0, J)$ are thermalized[37]. The factor $\alpha_{(u),l} \equiv A_{ul}/\Sigma_l A_{ul}$ is the probability to decay to state l given state u is excited, A_{ul} is Einstein coefficient for radiative decay, and E_{ul} is the energy of the transition. When cascade from high energy states is important, the level populations are coupled. However, for CR excitation of the low rotational levels of $v = 1$, direct impact dominates and the excitation rates simplify to $\zeta_{\mathrm{ex}} p_{u,(\mathrm{cr})}$. Values for E_{ul}, $\alpha_{(u),l}$, and $p_{u,(\mathrm{cr})}$ are presented Table 1. As discussed in Methods, in the case that the CRIR decreases with cloud depth, ζ_{ex} and ζ represent the CR excitation and ionization rates in cloud interiors.

The total brightness in all the emitted lines is

$$\begin{aligned} I_{\mathrm{tot},(\mathrm{cr})} &= \frac{1}{4\pi} g N_{\mathrm{H}_2} \varphi \zeta \bar{E}_{(\mathrm{cr})} \\ &= 3.6 \times 10^{-7} g N_{22} \zeta_{-16}\ \mathrm{erg\ cm^{-2}\ s^{-1}\ str^{-1}}, \end{aligned} \tag{3}$$

where $\zeta_{-16} \equiv \zeta/(10^{-16}\,\mathrm{s}^{-1})$, $\bar{E}_{(\mathrm{cr})} \equiv \sum_{ul} E_{ul} p_{u,(\mathrm{cr})} \alpha_{(u)l} \approx 0.486$ eV is the mean transition energy, and $\varphi \equiv \zeta_{ex}/\zeta \approx 5.8$ is the number of excitations per CR ionization (see Methods). The brightness in each individual line may be written as

$$I_{ul,(\mathrm{cr})} = f_{ul,(\mathrm{cr})} I_{\mathrm{tot},(\mathrm{cr})} \tag{4}$$

where

$$f_{ul,(\mathrm{cr})} \equiv p_{u,(\mathrm{cr})} \alpha_{(u)l} E_{ul} / \bar{E}_{(\mathrm{cr})}, \tag{5}$$

is the relative emission brightness.

The $f_{ul,(\mathrm{cr})}$ values for the brightest lines ($f_{ul,(\mathrm{cr})} > 0.1\%$) are presented in Table 1. The brightest lines (by far) are the (1-0) O (2), Q(2), S(0), O(4) transitions of para-H_2. These transitions are strong because the (v, J) = (1, 0), and (v, J) = (1, 2) states are

Table 1 H_2 line emission and excitation for excitation by cosmic-rays (CRs), ultraviolet (UV) radiation, and H_2 formation.

Transition	J_u	J_l	λ (μm)	E_{ul} (eV)	A_{ul} (10^{-7} s^{-1})	$\alpha_{(u),l}$	$p_{u,(cr)}$	$f_{ul,(cr)}$ (%)	$f_{ul,(uv)}$ (%)	$f_{ul,(f)}$ (%)		
										$\phi=1$	$\phi=2$	$\phi=3$
(1-0)O(2)	0	2	2.63	0.47	8.56	1.00	0.47	45.29	0.94	0.10	0.27	0.66
(1-0)Q(2)	2	2	2.41	0.51	3.04	0.36	0.47	17.67	1.01	0.17	0.34	0.88
(1-0)S(0)	2	0	2.22	0.56	2.53	0.30	0.47	15.99	0.91	0.16	0.30	0.80
(1-0)O(4)	2	4	3.00	0.41	2.91	0.34	0.47	13.57	0.78	0.13	0.26	0.67
(1-0)Q(1)	1	1	2.41	0.52	4.30	0.50	0.014	0.76	2.05	0.47	1.10	2.94
(1-0)S(1)	3	1	2.12	0.58	3.48	0.42	0.014	0.71	1.86	0.87	1.15	2.82
(1-0)O(3)	1	3	2.80	0.44	4.24	0.50	0.014	0.64	1.74	0.41	0.94	2.45
(1-0)Q(3)	3	3	2.42	0.51	2.79	0.33	0.014	0.50	1.31	0.61	0.84	1.96
(1-0)O(5)	3	5	3.23	0.38	2.09	0.25	0.014	0.28	0.74	0.35	0.46	1.09

H_2 Rovibrational transitions. The upper and lower states u and l have vibrational-rotational quantum numbers, $v_u=1$, $v_l=0$, and different J_u, J_l, as indicated. For each transition, λ_{ul}, E_{ul}, and A_{ul} are the transition wavelength, energy, and Einstein coefficient for spontaneous decay. $\alpha_{(u),l}\equiv A_{ul}/\sum_l A_{ul}$ is the probability to decay to state l given that state u is excited. $p_{u,(cr)}$ is the probability for populating state u, per CR excitation[37]. These values are weakly sensitive to the temperature for $T\lesssim 50$ K. $f_{ul,(cr)}=p_{u,(cr)}\alpha_{(u),l}\bar{E}_{ul}/\bar{E}_{(cr)}$ (with $\bar{E}_{(cr)}\approx 0.486$ eV) is the normalized line brightness, relative to the total line brightness for pure CR excitation. Correspondingly, $f_{ul,(uv)}$ and $f_{ul,(f)}$ are the normalized brightness for UV[31] and H_2 formation[33] excitation (normalized to the total line brightness for pure UV/formation excitation, respectively). For H_2 formation excitation, we considered three different H_2 formation models, $\phi=(1, 2, 3)$[30].

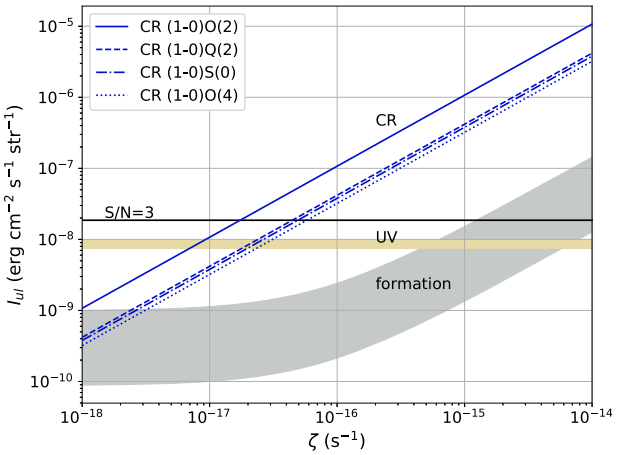

Fig. 1 Predicted energy surface brightness for the strongest rovibrational transitions, emitted from a molecular cloud of column density $N_{H_2}=10^{22}$ molecules per cm^2 that is exposed to the mean interstellar ultraviolet (UV) radiation field ($\chi=1$)[12], and to a cosmic-ray (CR) flux with an ionization rate ζ. Results are presented as functions of ζ (typically ζ is of order of 10^{-16} s^{-1}), and assuming either pure CR excitation (four diagonal lines), pure UV excitation (yellow horizontal strip) and pure H_2 formation excitation (grey strip). For UV pumping, the strip includes the four transitions. For formation pumping, it also encompasses the three different formation models, $\phi=1$, 2, 3[30]. The black horizontal line is the X-shooter sensitivity for a signal-to-noise ratio of 3, over 8 h integration time. For clouds with $\zeta >$ few 10^{-17} s^{-1}, the line emission is dominated by CR excitation and may be detected with a night integration time.

efficiently populated by direct impact excitation from the ground $(v, J)=(0, 0)$ state, while other levels are populated by radiative cascade[33,37]. Radiative cascade populates hundreds of levels, and thus the excitation efficiency for each individual level is low. The ortho-H_2 lines (odd J) are weak because the H_2 resides almost entirely in the para-H_2 ground state $(v, J)=(0, 0)$, and para-to-ortho conversion is inefficient. The ortho-lines become important in warmer gas (see Methods).

In Fig. 1 we show the strongest line brightness as a function of ζ, for $N_{22}=\chi=1$. The O(2) line is a factor of ~3 brighter than the other lines, Q(2), S(0), O(4), which are of comparable brightness. This is because there is equal probability for the excitation of both the $(v, J)=(1, 0)$ and $(v, J)=(1, 2)$ levels (i.e., equal p), but while the (1, 0) level is only allowed to decay to (0, 2), the (1, 2) level may decay to either (0, 2), (0, 0) or (0, 4). This is reflected in Table 1, where $\alpha=1$ for O(2) and $\alpha\approx 1/3$ for Q(2), S(0), and O(4). For this reason, $\bar{E}_{(cr)}\approx 0.486$ eV is so close to the energy of the O(2) line.

UV pumping. UV photons in the Lyman Werner (LW) band (11.2–13.6 eV) excite the H_2 electronic states, which cascade to the rovibrational levels of the ground electronic state. This UV pumping is effective in the cloud envelopes. With increasing cloud depth the radiation is attenuated by H_2 line absorption and dust absorption. Assuming H_2 formation-destruction (by photodissociation) steady-state, where H_2 destruction leads to H formation and using the fact that the H_2 pumping and photodissociation rates are proportional, the surface brightness in all the lines may be written as

$$I_{\rm tot,(uv)}=\frac{1}{4\pi}Rn\frac{P_0}{D_0}N_{\rm HI}\bar{E}_{\rm (uv)}, \tag{6}$$

see ref. [31] for a derivation of a related quantity (their Eq. (10)). In Eq. (6), R is the H_2 formation rate coefficient, n is the gas density, D_0 is the free-space H_2 photodissociation rate, $P_0\approx 9D_0$ is the UV pumping rate, and $\bar{E}_{\rm (uv)}\approx 1.82$ eV is the effective transition energy. We derived $\bar{E}_{\rm (uv)}$ by comparing Eq. (6) with Sternberg's[31] computations of $N_{\rm HI}$ and $I_{\rm tot,(uv)}$. The HI column density is

$$N_{\rm HI}=\frac{2\langle\mu\rangle}{\sigma_g}\ln\left(\frac{\alpha G}{4\langle\mu\rangle}+1\right), \tag{7}$$

where $\langle\mu\rangle\equiv\langle\cos(\theta)\rangle\approx 0.8$, $\sigma_g\equiv 1.9\times 10^{-21}\,\tilde{\sigma}$ cm^2 is the dust absorption cross section over the LW band, per hydrogen nucleus, and $\tilde{\sigma}$ is the cross-section in normalized units. $\alpha\equiv D_0/(Rn)$ and $G\approx 3.0\times 10^{-5}[9.9/(1+8.9\tilde{\sigma})]^{0.37}$ is a self-shielding factor[38,39]. Equation (7) assumes slab geometry and irradiation by isotropic UV field of strength $\chi/2$ on each of side of the slab. For beamed irradiation, multiply αG by 2 and set $\langle\mu\rangle=1$.

For densities $n/\chi\gtrsim 20$ cm^{-2}, $\alpha G\lesssim 3.2$, and we may expand Eq. (7), giving $N_{\rm HI}=\alpha G/(2\sigma_g)$, and

$$\begin{aligned} I_{\rm tot,(uv)} &\simeq \frac{P_0 G}{8\pi\sigma_g}\bar{E}_{\rm (uv)} \\ &\approx 9.6\times 10^{-7}\chi\ {\rm erg\ cm^{-2}\ s^{-1}\ str^{-1}}. \end{aligned} \tag{8}$$

where in the second equality we used $P_0=9D_0$, $D_0=5.8\times 10^{-11}\chi$ s^{-1} and $\tilde{\sigma}=1$. As long as $\chi/n<0.05$ cm^3, the brightness is independent of the density and the H_2 formation rate, and is proportional to the UV intensity, χ.

Given $I_{\rm tot,(uv)}$, the brightness in an individual line excited by UV is

$$I_{ul,(\rm uv)} = f_{ul,(\rm uv)} I_{\rm tot,(uv)}, \quad (9)$$

where the relative emissions, $f_{ul,(\rm uv)}$, are determined by the Einstein radiative decay coefficients. The $f_{ul,(\rm uv)}$ values are given in Table 1 based on Sternberg[31]. They are of order 1% and are much lower than the corresponding values for CR pumping. This is because UV pumping populates the levels through a cascade from electronic-excited-states, while for CR pumping, the levels are populated by direct impact excitation. Figure 1 shows the resulting line brightness at $\chi = 1$, and $N_{22} = 1$. Evidently, CR pumping dominates line emission for $\zeta_{-16} > 0.1 - 0.2$. More, generally, the ratio of emission arising from CR pumping relative to UV pumping is

$$\frac{I_{ul,(\rm cr)}}{I_{ul,(\rm uv)}} = 0.38 \frac{\zeta_{-16}}{\chi} \left(\frac{f_{ul,(\rm cr)}}{f_{ul,(\rm uv)}} \right) g N_{22}, \quad (10)$$

and the critical ζ/χ above which CR-pumping dominates is

$$\left(\frac{\zeta_{-16}}{\chi} \right)_{\rm c} = 2.7 \left(\frac{f_{ul,(\rm cr)}}{f_{ul,(\rm uv)}} g N_{22} \right)^{-1}. \quad (11)$$

For $N_{22} = 1$ ($g = 0.66$), $(\zeta_{-16}/\chi)_{\rm c} \approx 0.08$ for O(2), and ≈0.2 for Q(2), S(0), O(4).

Formation pumping. For each H_2 formed, a fraction of the binding energy is converted into level excitation. It is useful to separate the line emission by H_2 formation pumping into a sum of two components, the contributions from the molecular core in which H_2 is destroyed by CRs, and from the outer envelopes where UV photons destroy H_2. Assuming chemical steady state, the H_2 formation is proportional to H_2 destruction and we get

$$I_{\rm tot,(f,core)} = \frac{1}{4\pi} g N_{\rm H_2} y \zeta \bar{E}_{\rm (f)} \approx 1.7 \times 10^{-7} \varphi_E g N_{22} y \zeta_{-16} \ {\rm erg\ cm^{-2}\ s^{-1}\ str^{-1}}, \quad (12)$$

$$I_{\rm tot,(f,env)} = \frac{D_0 G}{8\pi\sigma_g} \bar{E}_{\rm (f)} \approx 7.6 \times 10^{-8} \varphi_E \chi \ {\rm erg\ cm^{-2}\ s^{-1}\ str^{-1}}, \quad (13)$$

for the inner core, and the outer envelopes, respectively. Here we defined $\varphi_E \equiv \bar{E}_{\rm (f)}/(1.3\,{\rm eV})$, where $\bar{E}_{\rm (f)} \approx 1.3$ eV corresponds excitation of the $v = 4$ level, as suggested by laboratory experiments[35], and the factor $y \approx 2$ accounts for additional removal of H_2 by H_2^+ in predominantly molecular gas (see Eq. 11 in [40]). Equations (12) and (13) have similar forms as Eqs. (3) and (8), as in the molecular core the H_2 removal rate is $\propto \zeta$, while in the outer envelopes removal is proportional to the UV pumping rate, $D_0 \propto P_0 \propto \chi$. The transition from core-to-envelope dominated formation pumping occurs when ζ/χ is smaller than

$$\left(\frac{\zeta_{-16}}{\chi} \right)_{\rm crit} = 0.46 (g N_{22} y)^{-1}, \quad (14)$$

where $gN_{22}y$ is typically of order unity.

The surface brightness of each line is

$$I_{ul,(\rm f)} = f_{ul,(\rm f)} I_{\rm tot,(f)}, \quad (15)$$

where $I_{\rm tot,(f)} = I_{\rm tot,(f,core)} + I_{\rm tot,(f,env)}$. The $f_{ul,(\rm f)}$ values are determined by the formation excitation pattern, which is uncertain. To illustrate the possible outcomes, we consider the three qualitatively different formation models, $\phi = 1$, 2, 3 explored by Black and Dishoeck[30] (see their Eqs. (2)–(4)). In Fig. 1 we show the resulting line brightness for H_2 formation pumping, for the four lines and the three formation models (grey strip), for $\chi = 1$. As expected, when $\zeta_{-16} \gtrsim 1$, $I_{ul,(\rm f)} \propto \zeta$ as the cloud core dominates formation pumping, while when $\zeta_{-16} \lesssim 1$, $I_{ul,(\rm f)}$ is independent of ζ.

However, importantly, in both limits H_2 formation pumping is never the dominant excitation mechanism. When $\zeta/\chi \gg (\zeta/\chi)_{\rm crit}$,

$$\frac{I_{ul,(\rm cr)}}{I_{ul,(\rm f)}} \approx 2.2 (y\varphi_E)^{-1} \left(\frac{f_{ul,(\rm cr)}}{f_{ul,(\rm f)}} \right). \quad (16)$$

Since $f_{ul,(\rm cr)} = 15$–45% and $f_{ul,(\rm f)} = 0.1 - 1\%$, CR pumping dominates line emission. When $\zeta/\chi \ll (\zeta/\chi)_{\rm crit}$, although formation-pumping may be more important than CR-pumping, it remains sub-dominant compared to UV pumping, as can be seen by comparing Eqs. (8) and (13). For formation-pumping to dominate over UV, the ratio $f_{ul,(\rm f)}/f_{ul,(\rm uv)}$ must be larger than $P_0/D_0 \approx 9$, which generally does not occur.

Continuum. The astronomical source for continuum radiation in the wavelength of interest is dominated by light reflected from interstellar dust grains[41]. Following[42], in the optically thin limit, the specific intensity in the K band is $I_{{\rm cont},\nu} \approx 8.0 \times 10^{-19} N_{22}$ erg cm^{-2} s^{-1} Hz^{-1} str^{-1}. Integrating over a spectral bin Δv (as the lines are narrow compared to Δv), and multiplying by the optical depth correction function, g, we get

$$I_{\rm cont} = 1.1 \times 10^{-8} g N_{22} R_4^{-1} \ {\rm erg\ cm^{-2}\ s^{-1} str^{-1}}, \quad (17)$$

where $R \equiv v/\Delta v$ is the resolving power, $R_4 \equiv R/10^4$, and where we used $v = 1.35 \times 10^{14}$ Hz corresponding to 2.2 μm.

Emission from small dust grains and polycyclic aromatic hydrocarbons (PAHs) heated by the interstellar UV field also contributes to the background continuum. Draine[36] have calculated the emission spectrum assuming a realistic dust population composed of amorphous silicates and carbonaceous grains of various sizes[43] and including the effect of temperature fluctuations of small grains and PAHs. At $\lambda = 2$–3 μm, they find $\lambda I_\lambda \approx 2 \times 10^{-27} N I_{\rm UV}$ erg s^{-1} str^{-1} per H nucleus. Assuming $I_{\rm UV} = 1$, $N = 10^{21}$ cm^{-2} (at higher columns the UV flux is exponentially absorbed by dust), and integrating over a spectral bin we get

$$I_{\rm cont,em} \approx 2 \times 10^{-10} R_4^{-1} \ {\rm erg\ cm^{-2}\ s^{-1}\ str^{-1}}, \quad (18)$$

Thus, at the wavelength of interest, dust emission is subdominant compared to scattered light.

Detectability. For ground based observations, Earth sky thermal (and line) emission is typically the dominant noise source. As a proof of concept we examine the detection feasibility with X-shooter on the Very Large Telescope (VLT) and focus on the S(0) and Q(2) lines (O(2) is blocked by the atmosphere and O(4) is outside X-shooter's range). We assume that the lines are narrow and the source is extended. For $\zeta_{-16} = N_{22} = 1$, the brightness of S(0) and Q(2) are $I = (3.8,\ 4.2) \times 10^{-8}$ erg cm^{-2} s^{-1} str^{-1}, respectively (Eqs. (3) and (4)). The estimated signal-to-noise ratio (SNR) per pixel for 1 h integration with the 0.4″ slit ($R = 11,600$), is $S/N = (0.29,\ 0.14)$ for S(0) and Q(2), respectively, (see Methods). For 8 h integration, and integrating along the slit (55 pixels), $S/N = (6.1,\ 2.9)$.

More generally, $S/N \propto \sqrt{tR\Delta\Omega}$, where $\Delta\Omega$ is the instrument's field of view (FoV). Nearby clouds extend over angles large compared to typical slit FoVs. For example, the dark cloud Barnard 68 has an angular radius ≈ 100″[44] and $\Omega_{\rm B68} \approx 30000$ arcsec^2, whereas the X-shooter slit FoV is only 11″ long and has $\Omega = 4.4$ arcsec^2. Longer slits will achieve better SNR, but the improvement is limited to a factor $\sqrt{18}$. The achieved SNR will also depend on the quality of flat-field correction and the level of signal homogeneity.

Substantial improvement may be achieved for instruments with non-slit geometry, e.g., integral field units, or narrowband filters, with large FoV. For example, for $\Omega = \Omega_{B68}$ the FoV solid angle is larger by a factor of $\approx$6800(compared to the 11″ slit), equivalent to an improvement of a factor $\sqrt{6800} \approx 82$ in the SNR. An alternative avenue is to use space-based observatories, such as the upcoming James Webb Space Telescope. From space, the noise in the IR is much lower, and at the same time the O(2) line, which is a factor of 4 brighter than S(0), is accessible (see Table 1).

Discussion

We presented an analytic study of H_2 rovibrational line formation produced by penetrating CRs, as well as by the competing processes: H_2 formation pumping, and UV pumping, and investigated the conditions required for (a) CRs to dominate line formation, and (b) for the lines to be sufficiently bright to be detected. We showed that in cold dense clouds, exposed to the mean UV field, the (1-0)O(2), Q(2), S(0), O(4) line emission is dominated by CR pumping, and thus detection of these lines may be used to constrain the CRIR.

Whether the lines are excited by CRs, UV, or formation pumping may be determined by the line ratios. For example, the ratio of 1-0 S (1) to 1-0 S(0) lines is $\approx$2 for UV excitation[30,31], and is in the range 3.5–5.6 for formation pumping[33]. On the contrary, for cold clouds excited by CRs, this ratio is predicted to be $\ll$1 (see Table 1).

Observations of the H_2 lines may be an efficient method to determine the CRIR in dense clouds. A survey of several clouds in various regions in the Galaxy may reveal the degree of fluctuations in the CRIR, while comparison with the CRIR in diffuse clouds (as probed by chemical tracers, e.g., H_3^+, ArH^+, etc.), may constrain the attenuation of CRs with cloud depth, and therefore the spectrum of low energy CRs[45]. Such tests may shed light on the nature and formation process of CRs in the Galaxy.

Methods

Relative line Brightness, f_{ul}. The line brightness following CR excitation depend on the excitation probabilities, $p_{u,(cr)}$. We derive $p_{u,(cr)}$ and φ based on data from[37], assuming $T = 30$ K and electron energy 30 eV. These authors presented data for the excitation to level u per CR ionization (rather than per CR excitation), denoted b_u—see their Table 2. Comparing our and their definitions, we get $p_{u,(cr)} = b_u\zeta/\zeta_{ex} = b_u/\varphi$, $\varphi \approx 5.8$.

For H_2 formation pumping, we obtain $f_{ul,(f)}$ for each of the three models $\phi = 1, 2, 3$ model based on[33]. We divided their reported line brightness by $I_{tot,\,f}$, as given by our Eqs. (12) and (13) with $N_{22} = 1$, $\chi = 0.58$, $\zeta_{-16} = 0.1$ appropriate to the assumed values in[33], and assuming $\varphi_E = (1.15, 3.5, 1.5)$ for $\phi = (1, 2, 3)$[30], respectively.

Gas temperature. In the results section, we focused on the low $T \lesssim 50$ K regime, typical of cold molecular cloud interiors. Here we discuss the case of warmer gas. We have carried out calculations for the line intensities as a function of temperature based on data from Gredel and Dalgarno[37] and Tine et al.[28]. Results for $T = 30$, 100, and 300 K are presented in Table 2. As long as $T < 60$ K, the spectrum is heavily dominated by the para-H_2 lines. In this limit the para-H_2 lines remain insensitive to T. This is because at these temperatures the H_2 molecules always reside mostly in the ground $(v, J) = (0, 0)$ state. For $T \gtrsim 60$ K, the $(v, J) = (0, 1)$ level is sufficiently populated such that CR pumping from this level effectively excites the $(v, J) = (1, 1)$ and (1, 3) states, resulting in emission of ortho-H_2 lines: S(1), Q (1), Q(3), O(3), and O(5). While the power in each individual transition is reduced, the total power summed over the lines is conserved.

Variation of ζ with cloud depth. In our Eqs. (3), (4), and (12) we assumed a constant CRIR. In practice, CRs interact with the gas leading to an attenuation of the CRIR with an increasing gas column. For columns $N = 10^{20} - 10^{25}$ cm^{-2}, the $\zeta - N$ relation may be described by a power law,

$$\zeta(N_{H_2}) = \zeta_0 \left(\frac{N_{H_2}}{N_0}\right)^{-a} \tag{19}$$

with $N_0 = 10^{20}$ cm^{-2}, and where the power-index a and the normalization ζ_0 depend on the spectrum of the CRs[45]. To account for a varying ζ, our expressions for the total line brightness should be modified as follows:

$$\zeta N_{H_2} \to \int_0^{N_{H_2}} \zeta(N_{H_2})\mathrm{d}N_{H_2} = \frac{\zeta_0 N_0}{1-a}\left(\frac{N_{H_2}}{N_0}\right)^{1-a} = \zeta(N_{H_2})N_{H_2}\frac{1}{1-a} \tag{20}$$

where we solved the integral assuming Eq. (20) with $a \neq 1$ (for the four CR spectra considered by[45], $a = 0.021$, 0.423, 0.04, 0.805).

Equation (20) shows that even in the case of a varying CRIR, our Eqs. (3), (4), and (12) still provide an excellent approximation for the line brightness, but with ζ representing the CRIR in cloud interior. The factor $1/(1-a)$ approaches unity for relatively flat spectra (i.e., models 1 and 2 in ref. [45]), and the brightness is then independent of the spectrum shape. If H_2 line observations are further combined with additional observations of the CRIR in diffuse cloud regions (e.g., with ArH^+, OH^+, H_2O^+; ref. [5]), the CR attenuation may be obtained, constraining the CR spectrum.

Line brightness dependence on ζ. Our Eq. (3) suggests that the line emission is linear in ζ. This relation holds as long as ζ is not too high. With increasing ζ both gas temperature increases (which affect the excitation pattern), and more importantly, the electron fraction, x_e increases. When $x_e \gtrsim 10^{-4}$, coulomb energy loses become substantial and line excitation is quenched (see Tables 2 and 3 in ref. [28]). However, this requires extreme CRIR, such that the gas is no longer molecular[8,40,46].

Collisional de-excitation. At sufficiently high density, collisional deexcitation (by thermal H_2, H, etc.) dominates over radiative decay, and the line emission is quenched. The critical density at which collisional de-excitation equals radiative decay is $n_{crit}(T) = A_{ul}/(x_{col}k_{ul\downarrow}(T))$, where A_{ul} is the Einstein coefficient for spontaneous emission, $k_{ul\downarrow}(T)$ is the collisional rate coefficient, and $x_{col} = n_{col}/n$ is the fractional abundance of the collision partner.

Let us estimate the critical density for $v = 1$–0 deexcitation in cold-dense clouds. For the $v = 1 \to 0$, $A_{ul} \approx (2\text{–}8) \times 10^{-7}$ s^{-1} (see Table 1). The rate coefficients at $T = 100$ K are of order of $k_\downarrow \approx 10^{-13}$ cm^3 s^{-1} and $k_\downarrow \approx 5 \times 10^{-18}$ cm^3 s^{-1}, for collisions with H and H_2, respectively[47,48]. In cloud interiors, the H/H_2 ratio is set by the balance of H_2 ionization by CRs and H_2 formation via dust catalysis. This gives $x_H/x_{H_2} \approx \zeta/(Rn) \approx 3.3 \times 10^{-5}\zeta_{-16}/(n_5 T_2^{0.5})$ where $R \approx 3 \times 10^{-17} T_2^{0.5}$ cm^3 s^{-1} is the H_2 formation rate coefficient, $T_2 \equiv T/(100\,\mathrm{K})$ and $n_5 \equiv n/(10^5 \mathrm{cm}^{-3})$ (for more details see §4.1 in ref. [40]). Hydrogen nucleus conservation ($x_H + 2x_{H_2} \simeq 1$) then implies $x_{H_2} \approx 0.5$, and $x_H \approx 1.7 \times 10^{-5}\zeta_{-16}/n_5$. For $T = 100$ K we obtain n_{crit} of order of 10^{11} cm^{-3}, both for collisions with H and H_2. In practice, the temperature in cloud cores is typically lower than 100 K leading to even lower collisional rates ($k_\downarrow$), and thus even higher critical densities. In conclusion, for the typical temperatures and densities in cold clouds ($T < 100$ K, $n \approx 10^4$–10^6 cm^{-3}), radiative decay strongly dominates over collisional deexcitation from the $v = 1$ levels.

Thermal excitation. In our model we ignored thermal (collisional) excitation. Although excitations by the non-thermal CRs occurs rarely (at a rate $\sim \zeta$), thermal excitation at $T \lesssim 100$ K is extremely negligible. The thermal excitation rate is $q = x_{col} n k_{ul\downarrow} \exp(-\Delta E_{ul}/(k_B T)) g_u/g_l$, where g_u, g_l are the quantum weights of the levels. While $x_{col}k_{ul\downarrow} \sim 10^{-18}$–$10^{-16}$ cm^3 s^{-1}, the exponential factor is $\sim 10^{-22}$ ($\Delta E_{ul}/k_B \approx 5500$ K). Thus, thermal excitation is negligible.

Exposure time calculator. For our estimation of the signal to noise ratio per pixel per hour integration, we used the X-shooter exposure time calculator provided in https://www.eso.org/observing/etc/bin/gen/form?INS.NAME=X-SHOOTER+INS.

Table 2 Cosmic-ray pumping—temperature dependence.

Transition	J_u	J_l	λ (μm)	$f_{ul,(cr)}$ (%)[a]		
				30 K[b]	100 K	300 K
(1-0)O(2)	0	2	2.63	45.29	16.41	9.69
(1-0)Q(2)	2	2	2.41	17.67	6.40	4.31
(1-0)S(0)	2	0	2.22	15.99	5.79	3.90
(1-0)O(4)	2	4	3.00	13.57	4.92	3.31
(1-0)Q(1)	1	1	2.41	0.76	15.34	17.76
(1-0)S(1)	3	1	2.12	0.71	14.37	16.64
(1-0)O(3)	1	3	2.80	0.64	12.97	15.02
(1-0)Q(3)	3	3	2.42	0.50	10.09	11.67
(1-0)O(5)	3	5	3.23	0.28	5.66	6.55

[a]Based on Gredel and Dalgarno[37], and Tine et al. [$x_e = 10^{-6}$].[28]
[b]The O(2), Q(2), S(0), and O(4) intensities are weakly sensitive to temperature at low T: they remain within 3% for $T < 34$ K, and within (10, 20, 30)% for $T <$ (41, 50, 58) K, respectively.

MODE=spectro, with the following setup. Emission Line: Lambda (2223.2, 2413.3) nm for S(0), Q(2) respectively. Flux (0.0089, 0.0098) × 10^{-16} erg s^{-1} cm^{-2} arcsec^2 for S(0), Q(2), respectively. FWHM = 0.093 nm (appropriate for a single spectral resolution element of the 0″.4 slit). Spatial distribution, Extended source. Moon FLI 0.5, Airmass 1.5, PWV 30 mm, Turbulence Category 70%. NIR slit width 0″.4, DIT = 900 s, NDIT = 4.

Data availability

The author declares that all data supporting the findings of this study is available within the paper.

Received: 9 October 2019; Accepted: 9 January 2020;
Published online: 07 February 2020

References

1. Grenier, I. A., Black, J. H. & Strong, A. W. The nine lives of cosmic rays in galaxies. *Ann. Rev. Astron. Astrophys.* **53**, 199 (2015).
2. Guelin, M., Langer, W. & Wilson, R. The state of ionization in dense molecular clouds. *Astron. Astrophys.* **107**, 107 (1982).
3. van der Tak, F. F. S. & van Dishoeck, E. F. Limits on the cosmic-ray ionization rate toward massive young stars. *Astron. Astrophys.* **358L**, 79V (2000).
4. Indriolo, N. & McCall, B. J. Investigating the cosmic-ray ionization rate in the galactic diffuse interstellar medium through observations of H_3^+. *Astrophys. J.* **745**, 91 (2012).
5. Neufeld, D. A. & Wolfire, M. G. The cosmic-ray ionization rate in the galactic disk, as determined from observations of molecular ions. *Astrophys J.* **845**, 163 (2017).
6. Bialy, S., Neufeld, D., Wolfire, M., Sternberg, A. & Burkhart, B. Chemical Abundances in a Turbulent Medium - H_2, OH^+, H_2O^+, ArH^+. *Astrophys J.* **885**, 109 (2019).
7. Gaches, B. A. L., Offner, S. S. R. & Bisbas, T. G. The astrochemical impact of cosmic rays in protoclusters. I. Molecular cloud chemistry. *Astrophys. J.* **878**, 105 (2019).
8. LePetit, F. et al. Physical conditions in the central molecular zone inferred by H3+. *Astron. Astrophys.* **585**, A105 (2016).
9. Indriolo, N. et al. Constraints on the cosmic-ray ionization rate in the $z \sim 2.3$ lensed galaxies SMM J2135-0102 and SDP 17b from observations of OH^+ and H_2O^+. *Astrophys. J.* **865**, 127 (2018).
10. Müller, H. S. P. et al. Detection of extragalactic argonium, ArH+, toward PKS 1830− 211. *Astronomy & Astrophysics* **582**, L4 (2015).
11. González-Alfonso, E. et al. Outflowing OH in Markarian 231: The Ionization Rate of the Molecular Gas. *The Astrophysical Journal* **857**, 66 (2018).
12. Dalgarno, A. The galactic cosmic ray ionization rate. *Proc. Natl Acad. Sci. USA* **103**, 12269 (2006).
13. Indriolo, N., McCall, B. J., Geballe, T. R. & Oka, T. H3+ in diffuse interstellar clouds: a tracer for the cosmic-ray ionization rate. *Astrophys. J.* **671**, 1736 (2007).
14. Crapsi, A., Caselli, P., Walmsley, M. C. & Tafalla, M. Observing the gas temperature drop in the high-density nucleus of L 1544. *Astron. Astrophys.* **470**, 221 (2007).
15. Glassgold, A. E., Galli, D. & Padovani, M. Cosmic-ray and X-ray heating of interstellar clouds and protoplanetary disks. *Astrophys. J.* **756**, 157 (2012).
16. Ivlev, A. V., Silsbee, K., Sipilä, O. & Caselli, P. Gas and dust temperature in pre-stellar cores revisited: new limits on cosmic-ray ionization rate. *Astrophys. J.* **884**, 176 (2019).
17. Caselli, P., Walmsley, C. M., Terzieva, R. & Herbst, E. The ionization fraction in dense clouds. *Astrophys. J.* **499**, 234 (1998).
18. Williams, J. P., Bergin, E. A., Caselli, P., Myers, P. C. & Plume, R. The ionization fraction in dense molecular gas. I. Low-mass cores. *Astrophys. J.* **503**, 689 (1998).
19. Kong, S., Caselli, P., Tan, J. C., Wakelam, V. & Sipilä, O. The deuterium fractionation timescale in dense cloud cores: A parameter space exploration. *Astrophys. J.* **804**, 1 (2015).
20. Shingledecker, C. N. et al. On the inference of the cosmic-ray ionization rate ζ from the HCO^+ -to-DCO^+ abundance ratio: the effect of nuclear spin. *Astrophys. J.* **830**, 151 (2016).
21. Sorochenko, R. L. & Smirnov, G. T. Detection of radio recombination lines of hydrogen ionized by cosmic-ray protons in the cool interstellar medium. *Astron. Rep.* **54**, 776 (2010).
22. Oonk, J. B. et al. Carbon and hydrogen radio recombination lines from the cold clouds towards Cassiopeia A. *Mon. Notices R. Astron. Soc.* **465**, 1066 (2017).
23. Yusef-Zadeh, F., Hewitt, J. W. & Wardle, M. et al. Interacting cosmic rays with molecular clouds: a bremsstrahlung origin of diffuse high-energy emission from the inner 2° × 1° of the Galactic center. *Astrophys. J.* **762**, 33 (2013).
24. Hollenbach, D. J. & Tielens, A. G. G. M. Photodissociation regions in the interstellar medium of galaxies. *Reviews of Modern Physics* **71**, 173-230, (1999).
25. Timmermann, R. et al. H2 infrared line emission from S140: a warm PDR. *Astron. Astrophys.* **315**, L281–L284 (1996)
26. Martini, P., Sellgren, K. & DePoy, D. L. Near-infrared spectroscopy of molecular hydrogen emission in four reflection nebulae: ngc 1333, ngc 2023, ngc 2068, and ngc 7023. *The Astrophysical Journal*, **526**, 772. (1999).
27. Draine, B. T. Photoelectric heating of interstellar gas. *Astrophys. J. Suppl. Ser.* **36**, 595 (1978).
28. Tine, S., Lepp, S., Gredel, R. & Dalgarno, A. Infrared response of H2 to X-rays in dense clouds. *Astrophys. J.* **481**, 282 (1997).
29. Dalgarno, A., Yan, M. I. N. & Liu, W. Electron energy deposition in a gas mixture of atomic and molecular hydrogen and helium. *ApJ* **125**, 237 (1999).
30. Black, J. H. & van Dishoeck, E. F. Fluorescent excitation of interstellar H2. *Astrophys. J.* **322**, 412 (1987).
31. Sternberg, A. The infrared response of molecular hydrogen gas to ultraviolet radiation - a scaling law. *Astrophys. J.* **332**, 400 (1988).
32. Sternberg, A. & Dalgarno, A. The infrared response of molecular hydrogen gas to ultraviolet radiation-High-density regions. *The Astrophysical Journal*, **338**, 197–233. (1989).
33. LeBourlot, J., des Forêts, G. P., Roueff, E., Dalgarno, A. & Gredel, R. Infrared Diagnostics of formation of H2 on interstellar dust. *Astrophys. J.* **449**, 178 (1995).
34. Tiné, S. et al. Observational indicators of formation excitation of H_2. *Astrophys. Space Sci.* **288**, 377 (2003).
35. Islam, F., Cecchi-Pestellini, C., Viti, S. & Casu, S. Formation pumping of molecular hydrogen in dark clouds. *Astrophys. J.* **725**, 1111 (2010).
36. Draine, B. T. Physics of the Interstellar and Intergalactic Medium. (Princeton University Press, 2011)
37. Gredel, R. & Dalgarno, A. Infrared response of H2 to X-rays. *Astrophys. J. Suppl. Ser.* 852 (1995).
38. Sternberg, A., Petit, F. L., Roueff, E. & Bourlot, J. L. HI-to-H2 transitions and H I column densities in galaxy star-forming regions. *Astrophys. J. Suppl. Ser.* **790**, 10S (2014).
39. Bialy, S. & Sternberg, A. Analytic H i-to-H2 photodissociation transition profiles. *Astrophys. J.* **822**, 83 (2016).
40. Bialy, S. & Sternberg, A. CO/H2, C/CO, OH/CO, and OH/O2 in dense interstellar gas: from high ionization to low metallicity. *Mon. Notices R. Astron. Soc.* **450**, 4424 (2015).
41. Foster, J. B. & Goodman, A. A. Cloudshine: new light on dark clouds. *Astrophys. J.* **636**, L105 (2006).
42. Padoan, P., Juvela, M. & Pelkonen, V.-M. High-resolution mapping of interstellar clouds by near-infrared scattering. *Astron. J.* **636**, 101 (2006).
43. Draine, B. T. & Li, A. Infrared emission from interstellar dust. IV. The silicate-graphite-PAH Model in the post-Spitzer era. *Astrophys. J.* **657**, 810 (2007).
44. Alves, J. F. Lada, C. J. & Lada, E. A. Internal structure of a cold dark molecular cloud inferred from the extinction of background starlight. *Nature* **409**, 159-161. (2001).
45. Padovani, M., Galli, D. & Glassgold, A. E. Cosmic-ray ionization of molecular clouds. *Astron. Astrophys.* **501**, 619 (2009).
46. Bayet, E., Williams, D. A., Hartquist, T. W. & Viti, S. Chemistry in cosmic ray dominated regions. *Mon. Notices R. Astron. Soc.* **414**, 1583 (2011).
47. Lique, F. Revisited study of the ro-vibrational excitation of H2 by H: towards a revision of the cooling of astrophysical media. *Mon. Notices R. Astron. Soc.* **453**, 810 (2015).
48. Flower, D. R. & Roueff, E. Rovibrational relaxation in collisions between H_2 molecules: II. Influence of the rotational state of the perturber. *J. Phys. B.* **32**, 3399 (1999).

Acknowledgements

S.B. thanks Alyssa Goodman, David Neufeld, Amiel Sternberg, Oren Slone, Brian McLeod, and Igor Chilingaryan for fruitful discussions.

Author contributions

The author carried out all the analytic derivations, numerical computations, and paper writing.

Competing interests

The author declares no competing interests.

Additional information

Supplementary information is available for this paper at https://doi.org/10.1038/s42005-020-0293-7.

Correspondence and requests for materials should be addressed to S.B.

Reprints and permission information is available at http://www.nature.com/reprints

Publisher's note Springer Nature remains neutral with regard to jurisdictional claims in published maps and institutional affiliations.